Original Research

Sphingosine-1-phosphate reduces adhesion of malignant mammary tumor cells MDA-MB-231 to microvessel walls by protecting endothelial surface glycocalyx

L. Zhang, M. Zeng, B. M. Fu[*]

Department of Biomedical Engineering, The City College of the City University of New York, 160 Convent Ave, New York, NY 10031

Correspondence to: fu@ccny.cuny.edu

Abstract: Sphingosine-1-phosphate (S1P) is a sphingolipid in plasma that plays a critical role in cardiovascular and immune systems. Endothelial surface glycocalyx (ESG) decorating the inner wall of blood vessels is a regulator of multiple vascular functions. To test the hypothesis that S1P can reduce tumor cell adhesion to microvessel walls by protecting the ESG, we quantified the ESG and MDA-MB-231 tumor cell adhesion in the presence and absence of 1μM S1P, and in the presence of the matrix metalloproteinase (MMP) inhibitor in post-capillary venules of rat mesentery. We also measured the microvessel permeability to albumin as an indicator for the microvessel wall integrity. In the absence of S1P, ESG was ~10% of that in the presence of S1P, whereas adherent tumor cells and the permeability to albumin and were ~3.5-fold (after 30 min adhesion) and ~7.7-fold that in the presence of S1P, respectively. In the presence of the MMP inhibitor, the results are similar to those in the presence of S1P. Our results conform to the hypothesis that protecting ESG by S1P inhibits MDA-MB-231 tumor cell adhesion to the microvessel wall.

Key words: Post-capillary venule in rat mesentery; Microvessel permeability to albumin; In situ immunostaining; Heparan sulfate; Matrix metalloproteinase.

Introduction

Tumor metastasis is the leading cause of cancer-related death among cancer patients (1, 2). To search for effective anti-metastatic therapies, many in vivo, ex vivo and in vitro studies have been conducted to understand underlying mechanism by which tumor cells interact with endothelial cells lining the microvessel wall for the adhesion and extravasation. The luminal surfaces of endothelial cells (ECs) that line our vasculature are covered by an endothelial surface glycocalyx layer (ESG), composed of proteoglycans, glycosaminoglycans (GAGs) and glycoproteins (3-6). The GAGs in the ESG are heparan sulfate (HS), hyaluronic acid (HA), chondroitin sulfate (CS) and sialic acid (SA), of which, the most abundant one is HS, accounting for 50–90% of the GAGs (4). This layer serves many vascular functions, including being a mechano-sensor and transducer (6, 7), maintaining vessel wall permeability (8-11) and modulating circulating blood cell-vessel wall interaction (3, 12-15). Recent study by Cai et al (2012) showed that tumor cell adhesion to the microvessel wall degrades ESG and increases microvessel permeability to a large molecule, albumin (16).

Sphingosine-1-phosphate (S1P), is a sphingolipid in plasma that plays a critical role in the cardiovascular and immune systems. Red blood cells (RBCs) are a major source of S1P in plasma, which acts continuously to maintain normal vascular permeability under physiological conditions (17-20). Serum albumin and high-density lipoprotein (HDL) carry ~90% of the S1P and both elicit the release of S1P from RBCs (20-22). Recent studies investigated S1P effects on hydraulic conductivity (Lp) and solute permeability (P) of intact post-capillary venules in rat mesentery (20, 23-28). These results showed that via receptor $S1P_1$, S1P can attenuate acute microvascular permeability increases by inflammatory agents such as platelet-activating factor (PAF) (23-25) and bradykinin (24, 26). In addition to attenuating increased microvessel permeability by inflammatory mediators, 1μM S1P decreased basal Lp by 63% for a group of vessels with slightly higher Lp (23) and by 30% for those with normal Lp (24). 1μM S1P also maintained normal albumin permeability in the absence of BSA in the perfusate (27).

To investigate the underlying structural mechanisms by which S1P maintains microvessel permeability, in an in vitro study using HMVEC (human dermal microvascular endothelial cells) monolayers, as well as in intact microvessels of rat mesentery, Adamson et al.(2010) found that S1P pretreatment inhibited rearrangements of VE-cadherin and occludin induced by PAF or bradykinin and preserved peripheral cortactin (24). In addition to endothelial junction proteins, endothelial surface glycocalyx (ESG) forms a barrier between blood circulation and the surrounding tissues and plays an important role in controlling microvessel permeability, especially microvessel permeability to large molecules. A recent study by Zeng et al (2014) using an in vitro cultured cell monolayer (rat fat-pad endothelial cells) has shown that S1P plays a critical role in protecting the ESG via the S1P1 receptor and inhibits the matrix metalloproteinase (MMP) activity-dependent shedding of heparan sulfate (HS), chondroitin sulfate (CS) and the ectodomain of syndecan-1 (29). Figure 1 demonstrates this molecular mechanism. More recent study in Zhang et al. (28)
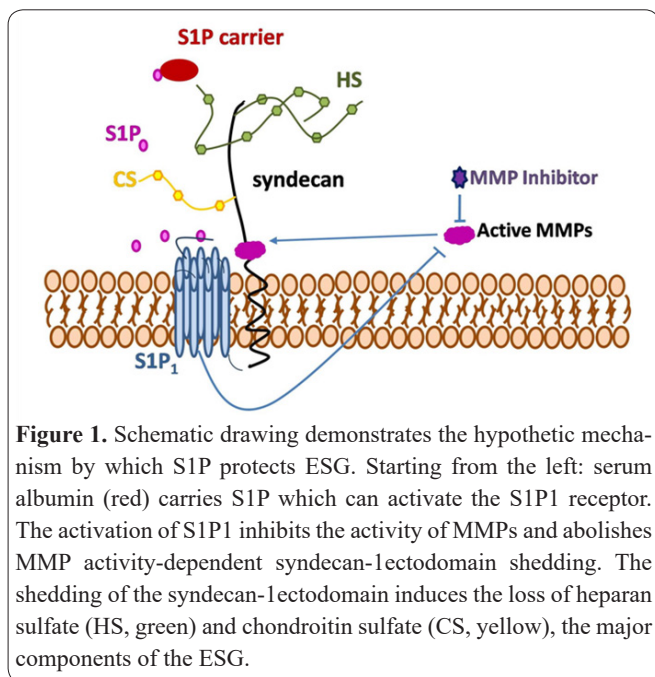
Figure 1. Schematic drawing demonstrates the hypothetic mechanism by which S1P protects ESG. Starting from the left: serum albumin (red) carries S1P which can activate the S1P1 receptor. The activation of S1P1 inhibits the activity of MMPs and abolishes MMP activity-dependent syndecan-1ectodomain shedding. The shedding of the syndecan-1ectodomain induces the loss of heparan sulfate (HS, green) and chondroitin sulfate (CS, yellow), the major components of the ESG.

confirmed the same role of S1P in protecting the ESG in vivo.

Increase in microvessel permeability is a critical step in many pathological processes including tumor cell adhesion to the microvessel wall (16, 30). The microvessel permeability or microvessel integrity is determined by the structural components of endothelial cells forming the microvessel wall (31). The structural components are ESG and endothelial junctions. Fu et al (2015) demonstrated that cAMP can enhance the endothelial junction integrity, decrease microvessel permeability and reduce tumor cell adhesion to the microvessel wall (30). To search for another approach to prevent tumor cell adhesion to microvessel walls, the aim of the present study was to test the hypothesis that S1P inhibits tumor cell adhesion to microvessel by preserving the ESG in intact microvessels. To test this hypothesis, the ESG in the post-capillary venules of rat mesentery was first quantified by immunostaining heparan sulfate (HS), the most abundant glycosaminoglycans (GAGs) of the ESG in the presence and absence of S1P, and in the presence of MMP inhibitors. Secondly, the adhesion rate of human malignant breast cancer cells MDA-MB-231 in the post-capillary venules was quantified in the presence and absence of S1P, and in the presence of MMP inhibitors. To further check the overall microvessel wall integrity, the microvessel solute permeability P to albumin (Stokes radius ~3.6 nm) was measured under the same conditions. By comparing the HS intensity of the ESG, MDA-MB-231 cell adhesion as well as permeability to BSA under these conditions, we concluded that S1P can inhibit tumor cell MDA-MB-231 adhesion to the microvessel wall by preserving the ESG and maintaining normal permeability to BSA.

Materials and Methods

Animal preparation

All experiments were performed on female Sprague-Dawley rats (250–300g), supplied by Hilltop Laboratory Animals (Scottsdale, PA). All procedures were approved by the Animal Care and Use Committees at the City College of the City University of New York. The methods used to prepare rat mesenteries, perfusate solutions, and micropipettes for microperfusion experiments have been described in detail in (16, 28, 32, 33).

Rats were first anaesthetized with pentobarbital sodium given subcutaneously. The initial dosage was 65 mg/kg, and an additional 3 mg/dose was given as needed. After a rat was anesthetized, a midline surgical incision (2–3 cm) was made in the abdominal wall. The rat was then transferred to a tray and kept warm on a heating pad. The mesentery was gently taken out from the abdominal cavity and spread on a glass coverslip, which formed the base of the observation platform as previously described (33). The gut was gently pinned out against a silicon elastomer barrier to maintain the spread of the mesentery. The upper surface of the mesentery was continuously superfused by a dripper with mammalian Ringer solution at 35–37°C, which was regulated by a controlled water bath and monitored regularly by a thermometer probe. The microvessels chosen for the study were post-capillary venules, with diameters of 35–50 μm. All vessels had brisk blood flow immediately before cannulation and had no marginating white cells. At the end of experiments, the animals were euthanized with excess anesthetic. The thorax was opened to ensure death.

Solutions and reagents

Mammalian Ringer solution was used for all dissections, perfusion, and superfusion. The solution compositions are (in mM) 132 NaCl, 4.6 KCl, 1.2 $MgSO_4$, 2.0 $CaCl_2$, 5.0 $NaHCO_3$, 5.5 glucose, and 20 HEPES. Its pH was balanced to 7.4 by adjusting the ratio of HEPES acid to base. In addition, the perfusate into the microvessel lumen contained fatty acid-free bovine serum albumin (BSA, A0281, Sigma, 66kDa, ~3.6 nm Stokes radius) at 10 mg/ml (1% BSA-Ringer solution). This fatty acid-free BSA has about 50 nM S1P (29), which is negligible compared to 1 μM S1P. FITC-conjugated mouse anti-human HS (anti-HS, $10e^4$ epitope) was purchased from United States Biological (Swampscott, MA). It was diluted to 1:50 (20 μg/ml) in 1% BSA-Ringer solution for labeling HS in the microvascular ESG (34). A blocking solution was made of 5% goat serum (Invitrogen, Eugene, OR) in 1% BSA-Ringer. All of the solutions described above were made at the time when the experiment was performed and were discarded at the end of the day. Sphingosine-1-phosphate (S1P) (73914, Sigma) was first dissolved in 95% methanol and prepared as a stock solution of 125 μM in 0.4% fatty acid-free BSA (29). A broad-spectrum hydroxamic acid inhibitor of MMPs, GM6001 and its negative control GM6001 NC were purchased from EMD Millipore.

To determine microvessel permeability to albumin, fatty acid-free bovine serum albumin was labeled with AlexaFluor 555 (Invitrogen) according to the manufacturer's instructions. The details for generating AlexFluor 555-BSA were described in (27, 28).

Cell culture

Human breast carcinoma cells (MDA-MB-231) from ATCC (Manassas, VA) were cultured in Dulbecco's Modified Eagle's Medium/Nutrient Mixture F-12 Ham (DMEM/F-12), 2 mM L-glutamine, and 100 U/

mL penicillin and 1 mg/mL streptomycin, all from Sigma-Aldrich, supplemented with 10% fetal bovine serum (FBS, Atlanta Biologicals, Flowery Branch, GA). All the cells were incubated in the humidified atmosphere with 5% CO_2 at 37 °C. On the day of experiment, MDA-MB-231 cells were collected by brief trypsinization, then counted and suspended in phosphate-buffered saline (PBS) (Sigma-Aldrich, St. Louis, MO). To remove any remaining cell clumps, the cell suspension was filtered through a 40μm nylon mesh. Then MDA-MB-231 cells were fluorescently labeled using 0.5μM Cell Tracker Red, EX/EM=577/602nm (Invitrogen, Eugene, OR) in serum-free DMEM medium for 30 min. Concentration of cell suspension was adjusted for the final perfusate ~4 million/ml in 1% BSA mammalian Ringer (35).

Intravital microscopy

A Nikon Eclipse TE2000-E inverted fluorescent microscope was used to observe the mesentery. A 10× lens (NA 0.3, Nikon) gave a field of view of approximately 2 mm in diameter. The tissue was observed with either transmitted white light from a light pipe suspended above the preparation or with fluorescent light from an illumination system (the monochromator with a xenon lamp FSM150Xe, Bentham Instrument Ltd., UK). The monochromator can generate the light of wavelength from 200 to 700 nm. The observation of fluorescently labeled glycocalyx and measurements of P to albumin were done by a high-performance digital 12-bit CCD camera (SensiCam QE, Cooke Corp., Romulus, MI, USA) with a Super Fluor 20x objective lens (NA=0.75, Nikon) and recorded by InCyt Im™ imaging and analyzing system (Intracellular Imaging Inc., Cincinnati, OH, USA).

Immuno-labeling and quantification of microvessel endothelial surface glycocalyx (ESG)

To compare the ESG of the microvessel wall in the presence or absence of S1P, FITC-conjugated heparan sulphate (HS) antibody was used to label HS, one of the most abundant glycosaminoglycans (GAGs) forming the ESG (6, 36). The detailed method was described in (26, 34). Briefly, a post-capillary venule was first cannulated with a single lumen micropipette with or without 1 μM S1P in the perfusate and perfused for 20 min. The upper surface of the mesentery was continuously superfused by a dripper with mammalian Ringer solution at 37°C, which was regulated by a controlled water bath and monitored by a thermometer probe. Then the cannulation was changed to a glass theta micropipette with two lumens. The vessel was first perfused for 15 min with a blocking solution of 5% goat serum in 1% BSA-Ringer (with or without S1P) through one lumen of the theta pipette. The superfusion temperature was gradually decreased to ~4°C in ~15 min. Then the perfusion was switched to another lumen of the pipette to inject FITC-conjugated anti-HS in 1%BSA-Ringer (20 mg/ml, with or without S1P) into the microvessels for ~2.5 h. After 15 min perfusion of the first perfusate to wash away the free dye, the vessel with fluorescently labeled glycocalyx (focused at the mid-plane of a vessel) was imaged by the same imaging system used in the P measurement. The intensity of the fluorescently labeled glycocalyx in the vessel segment was measured

offline by the InCyt Im™ imaging and analyzing system (Intracellular Imaging Inc., Cincinnati, OH, USA). To test the assumption that the fluorescence intensity is linearly related to the amount of the fluorescently labeled glycocalyx, we did in vitro calibration experiments. We used the same instrument settings in the calibration experiments as those used in the in vivo measurement of the fluorescently labeled glycocalyx. The linear range of FITC-anti-HS concentrations was from 0 to 50 mg/ml under our settings. We thus chose 20 mg/ml FITC-anti-HS in our experiments.

MDA-MB-231 cell adhesion in individually perfused microvessels

To measure the tumor cell adhesion rate under a controlled condition, a single straight post-capillary venule (35 to 50 μm diameter) was cannulated with a micropipette (~30 μm tip diameter, WPI, Sarasota, FL) filled with 1% BSA-Ringer solution containing ~4 million cells/ml. The venule was perfused with a driving pressure of ~10cmH$_2$O to maintain a flow velocity of ~1 mm/s, which is a typical blood flow velocity in the post-capillary venules of rat mesentery. The perfusion flow velocity was determined by the driving pressure and was calculated from the movement of a marker tumor cell (33). The rate of cells out of the micropipette was also measured, which was ~1 cell/s at the perfusion velocity of~1 mm/s. The adhesion process was recorded at ~2 frames/s in a ~1-min interval for ~30 min in each experiment. A single experiment was carried out in one microvessel per animal. Since 20x/numerical aperture (NA) 0.75 objective lens was used to observe the cell adhesion, which has a depth of light collection ~100 μm(37) , the cells adhering at the top and bottom of the vessel can also be observed when focusing at the midplane of the vessel. Due to the limitation of the two dimensional (2D) images, the midplane area was used as the projection of the surface area of the vessel where the cells adhere.

Measurement of microvessel solute permeability P

To further investigate if S1P maintains normal microvessel permeability, we measured apparent microvessel permeability (P) to a large solute, albumin (AlexFluor 555-BSA, ~3.6 nm Stokes radius) in the presence and absence of 1 μM S1P, and in the presence of a generic MMP inhibitor, GM6001 (10μM), or its negative control GM6001NC (10μM). Before P measurement, the microvessels were pretreated with these solutions for 20 min. These concentrations were the optimized concentrations used in (20, 23, 25, 29) for the S1P and inhibitor effects on the endothelial permeability in vivo and in vitro. The detailed method for P measurement has been previously described in (32, 33, 38). Briefly, a post-capillary venule was cannulated with a theta pipette. One lumen was filled with 1% BSA-Ringer (washout) and another lumen with the same solution additionally containing fluorescently labeled solutes (dye). When the dye solution was perfused into the vessel lumen, the vessel was exposed to 555nm wavelength light, the images were recorded simultaneously by a high-performance digital 12-bit charge-coupled device (CCD) camera (SensiCam QE, Cooke, Romulus, MI) with a Super Fluor x20 objective lens (NA =

0.75, Nikon). Then the P was determined offline. The total fluorescence intensity (I) in the lumen of a straight vessel and surrounding tissue was determined by image analysis software (Intracellular Imaging, Cincinnati, OH). The measuring window was 200-500 µm long and 100-200 µm wide and was set at least 100 µm from the cannulation site and from the base of the bifurcation to avoid solute contamination from the cannulation site and from the side arms. P was calculated by $P = (1/\Delta I_0)(dI/dt)_0(r/2)$, where ΔI_0 was the step increase in fluorescence intensity in the measuring window when the perfused dye just filled up the vessel lumen, $(dI/dt)_0$ was the initial rate of increase in fluorescence intensity after the dye filled the lumen and began to accumulate in the tissue, and r was the vessel radius. The assumption for using the above equation for determining the P was that the fluorescence intensity is linearly related to the fluorescence concentration. AlexFluor 555-BSA was at the concentration of 0.75 mg/ml, which was in the linear range under the imaging settings according to in vitro calibrations (28, 32, 38).

Determination of diffusive solute permeability P_d from measured apparent permeability P

The albumin P measured in our experiments (apparent P) tends to overestimate the true diffusive P (P_d) of albumin because solute flux can be coupled to water flow (solvent drag). Using the hydraulic conductivity Lp and reflection coefficient σ to albumin, which were measured under control and tumor cell adhesions (16), we calculated the P_d to albumin by employing the following formula in (32, 39, 40).

$$P = P_d \frac{P_e}{\exp(P_e) - 1} + L_p(1-\sigma)\Delta p_{eff} \quad (1)$$

$$P_e = \frac{L_p(1-\sigma)\Delta p_{eff}}{P_d} \quad (2)$$

$$\Delta p_{eff} = \Delta p - \sigma^{albu\,min}\Delta\pi^{albu\,min} - \sigma^{AlexF-albu\,min}\Delta\pi^{AlexF-albu\,min} \quad (3)$$

Here Δp_{eff} is the effective filtration pressure across the microvessel wall; Δp and $\Delta\pi$ are the hydrostatic and osmotic pressure drops across the microvessel wall, respectively, and Pe is the Peclet number. We assumed $\sigma^{albumin} = \sigma^{AlexF-albumin} = \sigma$ in our study.

Data analysis

Data are presented as means ± SE, unless indicated otherwise. Statistical analysis was performed by a T-test or two-way ANOVA using Sigma Plot 11.2 from Systat Software Inc. (San Jose, CA). A level of p < 0.05 was considered significant difference in all experiments.

Results

S1P protects ESG of the microvessel

To show that S1P can protect the ESG in intact microvessels as in cultured endothelial cells (29), the post-capillary venule was perfused in the presence or absence of 1 µM S1P in 1% BSA-Ringer for 20 mi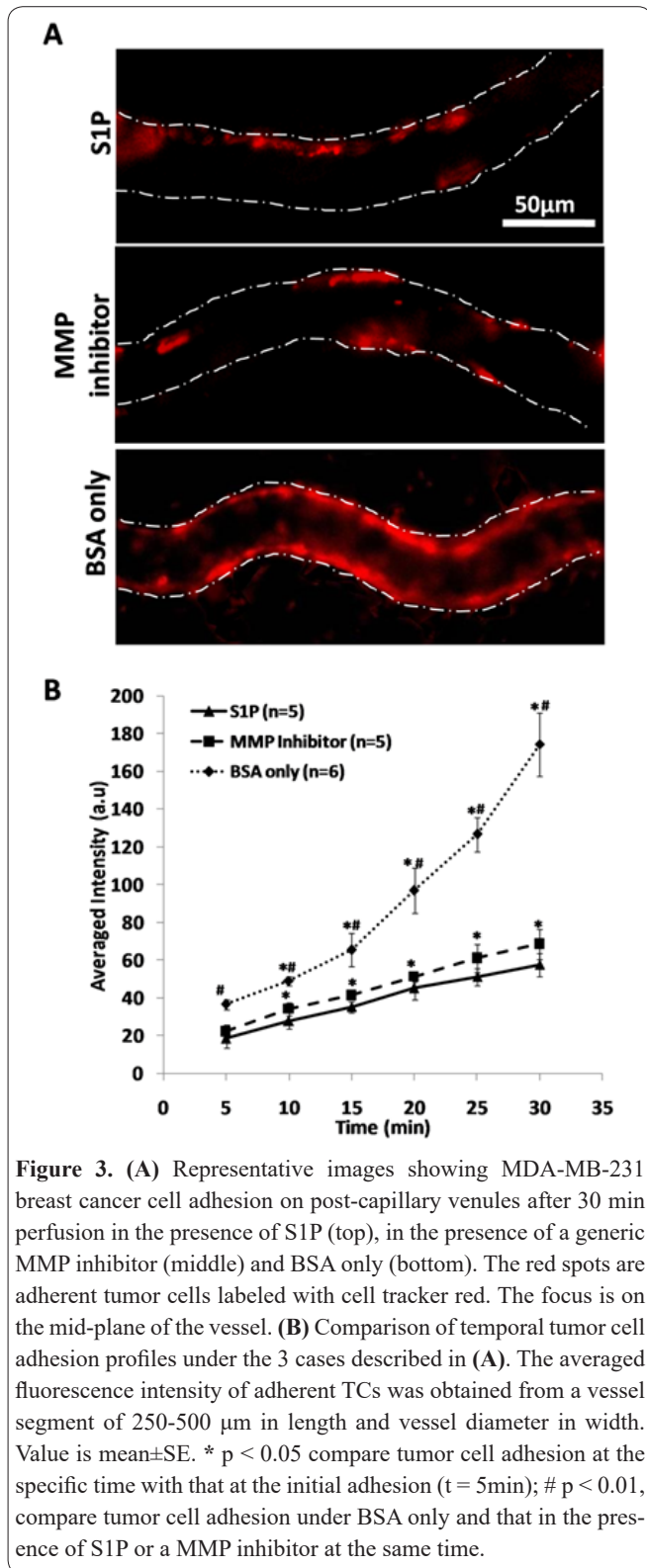n at 37°C degree. Then the microvessel ESG was quantified by immunolabeling HS, one of the most abundant GAGs in the ESG. Figure 2 shows the florescence images of the FITC-anti-HS labeled ESG in a post-capillary venule in the presence and absence of S1P and in the presence of a broad-spectrum MMP inhibitor. Figure 2A shows the mid-plane views of the FITC-anti-HS labeled ESG in the microvessels taken by our highly light-sensitive CCD camera. Since the 20x/NA0.75 objective lens was used to observe the ESG, which has a depth of light collection ~100 µm (37), the intensity of the FITC-anti-HS labeled ESG at the top and the bottom of the vessel can both be detected when we focus at the mid-plane of the vessel. The left image in Fig. 2A shows the FITC-anti-HS labeled ESG in the microvessel in the presence of S1P , the middle image is for that with the MMP inhibitor and the right image is for that in the absence of S1P. Figure 2B compares the intensity of the FITC-anti-HS labeled ESG under these three conditions. In the absence of S1P, the intensity of the FITC-anti-HS labeled ESG was only ~10% of that in the presence of S1P. In the absence of S1P but in the presence of the MMP inhibitor, the intensity of the FITC-anti-HS labeled ESG was 0.88 ± 0.11 of that in the presence of S1P (p = 0.56). S1P does protect the ESG in intact microvessels by inhibiting MMP activity.

Effect of S1P on MDA-MB-231 cell adhesion to post-capillary venules

To investigate whether S1P inhibits tumor cell adhesion to the microvessel wall via protecting the ESG, the MDA-MB-231 adhesion on post-capillary venules
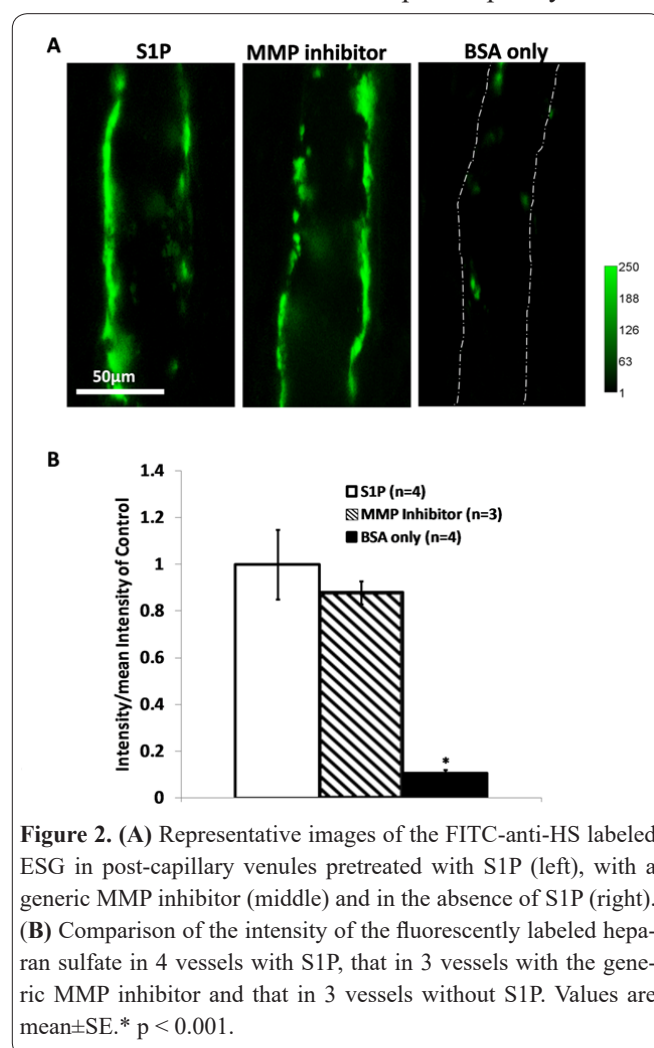
Figure 2. (A) Representative images of the FITC-anti-HS labeled ESG in post-capillary venules pretreated with S1P (left), with a generic MMP inhibitor (middle) and in the absence of S1P (right). **(B)** Comparison of the intensity of the fluorescently labeled heparan sulfate in 4 vessels with S1P, that in 3 vessels with the generic MMP inhibitor and that in 3 vessels without S1P. Values are mean±SE.* p < 0.001.

Figure 3. (A) Representative images showing MDA-MB-231 breast cancer cell adhesion on post-capillary venules after 30 min perfusion in the presence of S1P (top), in the presence of a generic MMP inhibitor (middle) and BSA only (bottom). The red spots are adherent tumor cells labeled with cell tracker red. The focus is on the mid-plane of the vessel. **(B)** Comparison of temporal tumor cell adhesion profiles under the 3 cases described in **(A)**. The averaged fluorescence intensity of adherent TCs was obtained from a vessel segment of 250-500 μm in length and vessel diameter in width. Value is mean±SE. ***** $p < 0.05$ compare tumor cell adhesion at the specific time with that at the initial adhesion ($t = 5$min); # $p < 0.01$, compare tumor cell adhesion under BSA only and that in the presence of S1P or a MMP inhibitor at the same time.

was quantified in the presence and absence of S1P and in the presence of the generic MMP inhibitor. Figure

3A shows the representative fluorescence images of the adherent cell-tracker red labeled MDA-MB-231 breast cancer cells in post-capillary venules after 30 min perfusion under various conditions. The top image is for that in the presence of S1P, the middle one for that in the presence of the generic MMP inhibitor and the bottom one for that in the absence of S1P. Figure 3B compares the temporal tumor cell adhesion profiles under these 3 conditions. Compared to that in the absence of S1P, in the presence of S1P or the generic MMP inhibitor the adherent tumor cells decreased as early as 5 min; at 30 min, the adherent tumor cells were ~33% and ~39% of that in the absence of S1P, respectively. These results conform to our hypothesis that S1P can inhibit TC adhesion to the microvessel wall by protecting the ESG via inhibition of MMP activity.

S1P maintains normal microvessel permeability

To further test whether S1P maintains normal microvessel permeability through protecting the ESG, the microvessel permeability P to albumin was measured in the presence and absence of S1P, and in the presence of the MMP inhibitor. The results were summarized in Table 1, which shows that after 20 min pretreatment with 1 μM S1P, P to albumin was $8.09 \pm 2.2 \times 10^{-7}$ cm/s (n=7), while in the absence of S1P, P increased by ~8.5-fold, to $68.8 \pm 7.6 \times 10^{-7}$ cm/s (n=7) ($p < 0.001$). Inhibition of MMPs reduced the P to $12.2 \pm 1.9 \times 10^{-7}$ cm/s (n=7), which has no significant difference from that in the presence of S1P ($p = 0.34$). However, the negative control of the MMP inhibitor did not reduce the P. Table 1 also shows the effect of solvent drag on permeability to albumin by using P from the measured values and L_p, σ to albumin from Cai et al, 2012 (16). We used
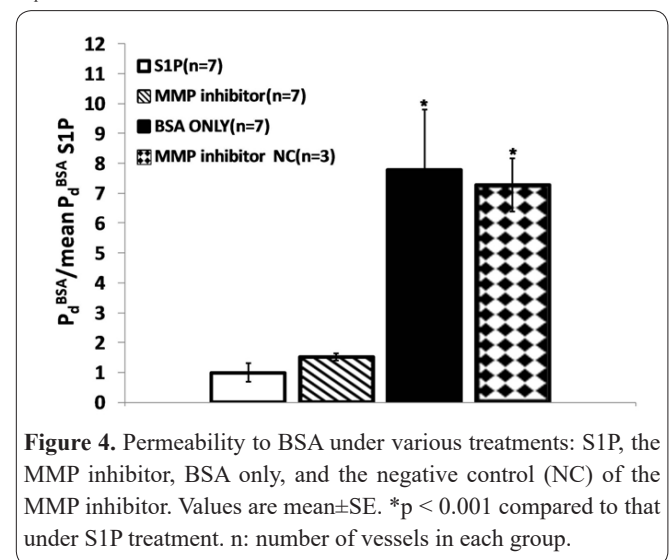

Figure 4. Permeability to BSA under various treatments: S1P, the MMP inhibitor, BSA only, and the negative control (NC) of the MMP inhibitor. Values are mean±SE. *$p < 0.001$ compared to that under S1P treatment. n: number of vessels in each group.

Table 1. Effect of solvent drag on P^{BSA} in the presence of S1P, in the presence of the MMP inhibitor, in the presence of the negative control of the MMP inhibitor, and BSA only in the perfusate.

	Δp_{eff} (cm H$_2$O)	$\sigma^{albumin\,\#}$	$L_p^{\#}$ (cm/s/cm H$_2$O)	P^{BSA} (cm/s)	P_e	P_d (cm/s)
S1P	10	0.940	1.1×10^{-7}	8.09×10^{-7}	0.09	7.75×10^{-7}
MMP inhibitor	10	0.940	1.1×10^{-7}	12.2×10^{-7}	0.06	11.87×10^{-7}
BSA only	10	0.423	2.8×10^{-7}	68.8×10^{-7}	0.27	60.04×10^{-7}
MMP NC	10	0.423	2.8×10^{-7}	64.9×10^{-7}	0.29	56.44×10^{-7}

The value of $\sigma^{albumin}$ and L_p are from Cai et al. (2012).

Eqs. (1)-(3) to calculate the P_d to albumin, which was 7.75×10^{-7} cm/s in the presence of S1P, 11.87×10^{-7} cm/s in the presence of the MMP inhibitor, 60.04×10^{-7} cm/s in the absence of S1P and 56.44×10^{-7} cm/s in the presence of the negative control of the MMP inhibitor. Figure 4 plots the relative diffusive permeability P_d to that in the presence of S1P under these conditions. Our results demonstrate that S1P maintains normal microvessel permeability by inhibiting MMP activity, the consequence of protecting the ESG.

Discussion

Tumor cell adhesion to the microvessel wall is one of the critical steps in tumor metastasis (2). Exploring new approaches to prevent tumor cell adhesion to endothelium lining is important in developing anti-metastatic strategies. Thus the aim of this study was to determine the effect of S1P on microvessel integrity in intact microvessels and its role in tumor cell adhesion.

It is well established that the ESG contains a wide variety of membrane-bound carbohydrate-rich macromolecules including sulfated proteoglycans and glycosaminoglycans (GAGs). Due to its composition and unique location at the interface of circulating blood and the vessel wall, this ESG plays an important role in maintaining vascular permeability, attenuating interactions between circulating blood cells and the endothelial cells forming the vessel wall, as well as sensing the hydrodynamic changes in the blood flow (4, 6, 9, 12-14, 41, 42). As shown in Figure 1, syndecans are one of the major proteoglycans found in ESG, which anchor GAGs to the endothelial cell cytoskeleton, membrane and cytoplasm. GAGs are further categorized as heparan sulfate (HS), chondroitin sulfate (CS), dermatan sulfate, keratin sulfate and hyaluronic acid or hyaluronan (HA) (4, 41, 43). HS is the most abundant one, which is ~50-90% of the total GAGs (4, 43). Our newly developed technique of in situ immunolabeling of HS, CS and HA in intact post-capillary venules of rat mesentery (16, 34) revealed that compared to HS, the amount of CS and HA can be neglected in these microvessels (7). By employing this newly developed technique for in situ immunostaining of the ESG in an individual microvessel and the measurement of microvessel solute permeability in the same type of intact microvessels in the presence and absence of S1P, we have confirmed that S1P contributes to the maintenance of normal vascular permeability by protecting the ESG in intact microvessels (28).

The cellular mechanisms by which S1P acts to enhance endothelial barrier functions both in vivo and in vitro were thought to be via S1P1 ligation(20, 23, 25, 29, 44-46). Ligation of S1P1 receptor activates the Rho family small GTPase Rac 1, leading to peripheral localization of cytoskeletal effectors such as cortactin. This localization promotes adherens junction and tight junction formation (24), which promotes cell-cell adhesion and cell-substrate adhesion, resulting in enhancing endothelial barrier function. Via S1P1 receptor, another mechanism of S1P action is to stabilize the endothelial surface glycocalyx (ESG) by reducing matrix metalloproteinase (MMP) activation and attenuating the loss of ESG (29). Our in situ immunolabeling of the ESG

directly showed that S1P can preserve the ESG in intact microvessels (Fig. 2), the same as that observed in cultured endothelial cell monolayers (29).

To test the effect of S1P on preventing tumor adhesion to microvessel walls, the MDA-MB-231 breast cell adhesion rate was measured in the absence and presence of S1P, and in the presence of a MMP inhibitor. These experiments have shown that S1P does inhibit tumor cell MDA-MB-231 adhesion by over 60% in 30 min. Preserving the ESG of the microvessel wall by S1P not only reduces the interaction between cell adhesion molecules (CAMs) at tumor cells MDA-MB-231 and those at endothelial cells lining the microvessel wall, but also prevents tumor cell MDA-MB-231 adhesion to the CAMs in the ECM of endothelium (33, 47), resulting in reduction of tumor cell MDA-MB-231 adhesion to the microvessel walls.

In summary, we have shown in this study that S1P can reduce breast carcinoma MDA-MB-231 cells to microvessel walls by protecting the ESG. Our results thus suggest a new anti-tumor metastatic therapy via ESG protection.

References

1. Gassmann P and Haier J. The tumor cell-host organ interface in the early onset of metastatic organ colonisation. Clin Exp Metastasis 2008; 25: 171-181.

2. Steeg PS. Tumor metastasis: mechanistic insights and clinical challenges. Nat Med 2006; 12: 895-904.

3. Barakat AI. Dragging along: the glycocalyx and vascular endothelial cell mechanotransduction. Circulation Research 2008; 102: 747-748.

4. Tarbell JM and Pahakis MY. Mechanotransduction and the glycocalyx. Journal of internal medicine 2006; 259: 339-350.

5. Weinbaum S, Tarbell JM and Damiano ER. The structure and function of the endothelial glycocalyx layer. Annual review of biomedical engineering 2007; 9: 121-167.

6. Fu BM and Tarbell JM. Mechano-sensing and transduction by endothelial surface glycocalyx: composition, structure, and function. Wiley Interdiscip Rev Syst Biol Med 2013; 5: 381-390.

7. Yen WY, Cai B, Yang JL, Zhang L, Zeng M, Tarbell JM and Fu BM. Endothelial Surface Glycocalyx Can Regulate Flow-Induced Nitric Oxide Production in Microvessels In Vivo. PLoS One. 2015; 9;10(1):e0117133.

8. Becker BF, Chappell D and Jacob M. Endothelial glycocalyx and coronary vascular permeability: the fringe benefit. Basic research in cardiology 2010; 105: 687-701.

9. Curry FR and Adamson RH. Vascular permeability modulation at the cell, microvessel, or whole organ level: towards closing gaps in our knowledge. Cardiovascular research 2010; 87: 218-229.

10. van den Berg BM, Vink H and Spaan JA. The endothelial glycocalyx protects against myocardial edema. Circulation Research 2003; 92: 592-594.

11. van Haaren PM, VanBavel E, Vink H and Spaan JA. Localization of the permeability barrier to solutes in isolated arteries by confocal microscopy. American journal of physiology. Heart and circulatory physiology 2003; 285: H2848-2856.

12. Constantinescu AA, Vink H and Spaan JA. Endothelial cell glycocalyx modulates immobilization of leukocytes at the endothelial surface. Arteriosclerosis, thrombosis, and vascular biology 2003; 23: 1541-1547.

13. Mulivor AW and Lipowsky HH. Inhibition of glycan shedding and leukocyte-endothelial adhesion in postcapillary venules by sup-

pression of matrixmetalloprotease activity with doxycycline. Microcirculation 2009; 16: 657-666.

14. Pries AR, Secomb TW and Gaehtgens P. The endothelial surface layer. Pflugers Archiv : European journal of physiology 2000; 440: 653-666.

15. Wu Q, Andreopoulos Y and Weinbaum S. From red cells to snowboarding: a new concept for a train track. Physical Review Letters 2004; 93: 194501.

16. Cai B, Fan J, Zeng M, Zhang L and Fu BM. Adhesion of malignant mammary tumor cells MDA-MB-231 to microvessel wall increases microvascular permeability via degradation of endothelial surface glycocalyx. Journal of Applied Physiology 2012; 113: 1141-1153.

17. Hanel P, Andreani P and Graler MH. Erythrocytes store and release sphingosine 1-phosphate in blood. FASEB J 2007; 21: 1202-1209.

18. Bouma HR, Kroese FG, Kok JW, Talaei F, Boerema AS, Herwig A, Draghiciu O, van Buiten A, Epema AH, van Dam A, Strijkstra AM and Henning RH. Low body temperature governs the decline of circulating lymphocytes during hibernation through sphingosine-1-phosphate. Proc Natl Acad Sci U S A 2011; 108: 2052-2057.

19. Bode C SS, Peest U, Beutel G, Thol F, Levkau B, Li Z, and Bittman R HT, Tolle M, van der Giet M, Graler MH. Erythrocytes serve as a reservoir for cellular and extracellular sphingosine 1-phosphate. Journal of Cellular Biochemistry 2010; 109: 1232-1243.

20. Curry FE, Clark JF and Adamson RH. Erythrocyte-derived sphingosine-1-phosphate stabilizes basal hydraulic conductivity and solute permeability in rat microvessels. Am J Physiol Heart Circ Physiol 2012; 303: H825-834.

21. Ohkawa R, Nakamura K, Okubo S, Hosogaya S, Ozaki Y, Tozuka M, Osima N, Yokota H, Ikeda H and Yatomi Y. Plasma sphingosine-1-phosphate measurement in healthy subjects: close correlation with red blood cell parameters. Ann Clin Biochem 2008; 45: 356-363.

22. Hla T. Physiological and pathological actions of sphingosine 1-phosphate. Semin Cell Dev Biol 2004; 15: 513-520.

23. Minnear FL, Zhu L and He P. Sphingosine 1-phosphate prevents platelet-activating factor-induced increase in hydraulic conductivity in rat mesenteric venules: pertussis toxin sensitive. Am J Physiol Heart Circ Physiol 2005; 289: H840-844.

24. Adamson RH, Sarai RK, Altangerel A, Thirkill TL, Clark JF and Curry FR. Sphingosine-1-phosphate modulation of basal permeability and acute inflammatory responses in rat venular microvessels. Cardiovascular research 2010; 88: 344-351.

25. Zhang G, Xu S, Qian Y and He P. Sphingosine-1-phosphate prevents permeability increases via activation of endothelial sphingosine-1-phosphate receptor 1 in rat venules. Am J Physiol Heart Circ Physiol 2010; 299: H1494-1504.

26. Adamson RH, Sarai RK, Clark JF, Altangerel A, Thirkill TL and Curry FE. Attenuation by sphingosine-1-phosphate of rat microvessel acute permeability response to bradykinin is rapidly reversible. Am J Physiol Heart Circ Physiol 2012; 302: H1929-1935.

27. Adamson RH, Clark JF, Radeva M, Kheirolomoom A, Ferrara KW and Curry FE. Albumin modulates S1P delivery from red blood cells in perfused microvessels: mechanism of the protein effect. Am J Physiol Heart Circ Physiol 2014; 306: H1011-1017.

28. Zhang L, Zeng M, Fan J, Tarbell JM, Curry FR and Fu BM. Sphingosine-1-phosphate Maintains Normal Vascular Permeability by Preserving Endothelial Surface Glycocalyx in Intact Microvessels. Microcirculation 2016; 23: 301-310.

29. Zeng Y, Adamson RH, Curry FR and Tarbell JM. Sphingosine-1-phosphate protects endothelial glycocalyx by inhibiting syndecan-1 shedding. American journal of physiology. Heart and circulatory physiology 2014; 306: H363-372.

30. Fu BM, Yang J, Cai B, Fan J, Zhang L and Zeng M. Reinforcing endothelial junctions prevents microvessel permeability increase and tumor cell adhesion in microvessels in vivo. Sci Rep 2015; 5: 15697.

31. Masako Sugihara-Sekia and Fu BM. Blood flow and permeability in microvessels. Fluid Dynamics Research 2005; 37: 82-132.

32. Fu BM and Shen S. Acute VEGF effect on solute permeability of mammalian microvessels in vivo. Microvasc Res 2004; 68: 51-62.

33. Shen S, Fan J, Cai B, Lv YG, Zeng M, Hao YY, Giancotti FG and Fu BMM. Vascular endothelial growth factor enhances cancer cell adhesion to microvascular endothelium in vivo. Experimental physiology 2010; 95: 369-379.

34. Yen WY, Cai B, Zeng M, Tarbell JM and Fu BM. Quantification of the endothelial surface glycocalyx on rat and mouse blood vessels. Microvasc Res. 2012;83(3):337-46.

35. Zhang L, Zeng M and Fu BM. Inhibition of endothelial nitric oxide synthase decreases breast cancer cell MDA-MB-231 adhesion to intact microvessels under physiological flows. Am J Physiol Heart Circ Physiol 2016; 310: H1735-1747.

36. Reitsma S, oude Egbrink MG, Vink H, van den Berg BM, Passos VL, Engels W, Slaaf DW and van Zandvoort MA. Endothelial glycocalyx structure in the intact carotid artery: a two-photon laser scanning microscopy study. J Vasc Res 2011; 48: 297-306.

37. Yuan W, Lv YG, Zeng M and Fu BM. Non-invasive measurement of solute permeability in cerebral microvessels of the rat. Microvascular Research 2009; 77: 166-173.

38. Liu Q, Zeng M and Fu BM. Microvascular hyperpermeability and thrombosis induced by light/dye treatment. Biomech Model Mechanobiol 2011; 10: 235-247.

39. Curry PE HV, Sarelius IH, *Cardiovascular Physiology. Techniques in the Life Sciences*, Elsevier, New York (1983).

40. Fu BM and Shen S. Structural mechanisms of acute VEGF effect on microvessel permeability. Am J Physiol Heart Circ Physiol 2003; 284: H2124-2135.

41. Reitsma S, Slaaf DW, Vink H, van Zandvoort MA and oude Egbrink MG. The endothelial glycocalyx: composition, functions, and visualization. Pflugers Archiv : European journal of physiology 2007; 454: 345-359.

42. Curry FR and Noll T. Spotlight on microvascular permeability. Cardiovascular research 2010; 87: 195-197.

43. Oohira A, Wight TN and Bornstein P. Sulfated proteoglycans synthesized by vascular endothelial cells in culture. J Biol Chem 1983; 258: 2014-2021.

44. Garcia JG, Liu F, Verin AD, Birukova A, Dechert MA, Gerthoffer WT, Bamberg JR and English D. Sphingosine 1-phosphate promotes endothelial cell barrier integrity by Edg-dependent cytoskeletal rearrangement. J Clin Invest 2001; 108: 689-701.

45. McVerry BJ and Garcia JG. Endothelial cell barrier regulation by sphingosine 1-phosphate. J Cell Biochem 2004; 92: 1075-1085.

46. Wang L and Dudek SM. Regulation of vascular permeability by sphingosine 1-phosphate. Microvasc Res 2009; 77: 39-45.

47. Fan J, Cai B, Zeng M, Hao Y, Giancotti FG and Fu BM. Integrin beta4 signaling promotes mammary tumor cell adhesion to brain microvascular endothelium by inducing ErbB2-mediated secretion of VEGF. Ann Biomed Eng 2011; 39: 2223-2241.